Improving Molecular Arrangement and Alleviating Nonradiative Energy Loss Using a Chlorinated Pyrido[3,4-*b*]quinoxaline-Core-Based Acceptor for High-Performance Organic Solar Cells

Han Tian, Yongmin Luo, Zhanxiang Chen, Tongle Xu*, Ruijie Ma*, Jiaying Wu*, Gang Li*, Chuluo Yang, Zhenghui Luo*

H. Tian, Z. Chen, T. Xu, C. Yang, Z. Luo
Guangdong Provincial Key Laboratory of New Energy Materials Service Safety, Shenzhen Key Laboratory of New Information Display and Storage Materials, College of Materials Science and Engineering, Shenzhen University, Shenzhen 518060, China.
Email: xutongletaylor@163.com; zhhuiluo@szu.edu.cn.

Y. Luo, J. Wu
Function Hub, Advanced Materials Thrust, The Hong Kong University of Science and Technology (Guangzhou), Nansha, Guangzhou, 511400, China. Email: jiayingwu@hkust-gz.edu.cn.

R. Ma, G. Li
Department of Electrical and Electronic Engineering, Research Institute for Smart Energy (RISE), Photonic Research Institute (PRI), The Hong Kong Polytechnic University, Hong Kong, 999077, China. Email: ruijie.ma@polyu.edu.hk; gang.w.li@polyu.edu.hk.

Abstract

The electron-deficient A_1 unit in A-DA_1D-A structured acceptors is critical for optimizing the efficiency of organic solar cells (OSCs). Drawing inspiration from the high performance of our previously reported pyrido[2,3-*b*]quinoxaline-core acceptors, we designed Py6, an isomer of Py1 with a repositioned pyridine nitrogen atom, and further modified it by chlorinating Py6 to create Py7. Theoretical calculations show that chlorine incorporation strengthens intermolecular non-covalent interactions and promotes the tighter molecular stacking, as confirmed by grazing-incidence wide-angle X-ray scattering. Consequently, D18/Py7 device delivers the enhanced fill factor and short-circuit current density, compared to D18/Py1 and D18/Py6 device. Notably, D18/Py7 device also yields a higher open-circuit voltage of 0.871 V, significantly outperforming Py1 (0.764 V) and Py6 (0.723 V), due to the low nonradiative energy losses. Further studies reveal that introducing Cl directs hole density toward the central pyrido[3,4-*b*]quinoxaline unit and decreases the charge transfer state ratio of D18/acceptor. This prompts triplet-to-singlet conversion and reduces non-radiative recombination losses. Additionally, using a mutual donor-acceptor dilution strategy, the (D18:1wt% Py7)/(Py7:1wt% D18) device achieves an impressive efficiency of 19.60%. Our work emphasizes the great potential of the Py-series acceptors and demonstrates that chlorine incorporation effectively reduces non-radiative losses.

Keywords: organic solar cells; power conversion efficiency; small-molecule acceptors; molecular packing; nonradiative energy loss

Introduction

Thanks to a deeper understanding of molecular design and device technology, organic solar cells (OSCs) have made considerable strides in the past decade.[1-12] In terms of device technology, both ternary and tandem devices have proven to be effective in improving the power conversion efficiency (PCE) of PSCs.[13-25] On the molecular design front, it is easy to associate with the recent emergence of acceptor-donor-acceptor (A-D-A) typed small-molecule acceptors (SMAs).[26-32] Notably, the A-D-A typed SMAs have achieved remarkable success, with OSCs based on Y6-like (a special A-D-A structure, namely A-DA$_1$D-A structure) SMAs reaching PCEs of over 20%.[33-38]

Inspired by the excellent photovoltaic efficiency of A-DA$_1$D-A type acceptors, ongoing research is focused on optimizing their molecular structures by modifying side chains, end groups and the central core with the aim of achieving further breakthroughs in device efficiency. Among these efforts, acceptors featuring quinoxaline (Qx) as electron-deficient units have recently attracted significant attention for the following reasons: i. Compared with the commonly used electron-deficient benzothiadiazole (BT) unit, the Qx unit, when employed as a central electron-deficient component, provides a molecular synthesis template for central core expansion, aiding in the fine-tuning of the material's aggregation and crystallization behavior;[39-42] ii. Qx-based acceptors can suppress electron-phonon coupling, enhance luminescence efficiency, and reduce reorganization energy, thereby achieving low non-radiative energy loss;[43-47] iii. Due to the relatively weak electron-withdrawing ability of Qx, its incorporation raises the lowest unoccupied molecular orbital (LUMO) energy level, which enlarges the energy level offset between the donor's highest occupied molecular orbital (HOMO) and the acceptor's LUMO, ultimately contributing to a higher open-circuit voltage (V_{OC}).[48-50]

Recently, we developed a series of five pyrido[2,3-*b*]quinoxaline-based SMAs (Py1-Py5), among which Py2 achieved the highest device efficiency of 17.73%, owing to better charge transport and more favorable morphology. However, a key point overlooked in this study is that the device based on mono-chlorinated Py2 exhibited a significantly higher V_{OC} of 0.871 V, compared to the unchlorinated Py1-based device, which had a V_{OC} of 0.736 V.[27] In this work, to further investigate the photovoltaic potential of the Py-series acceptors and to determine whether the V_{OC} enhancement upon chlorination is consistent across this system, we developed Py6, an isomer of Py1 with the pyridine nitrogen atom repositioned, and then chlorinated Py6 to create Py7. According to density functional theory (DFT) results, Py7 exhibits more compact dimer stacking and longer LUMO overlap lengths compared to the non-chlorinated Py1 and Py6. Grazing-incidence wide-angle X-ray

scattering (GIWAXS) further confirms that Py7 shows enhanced molecular packing and improved crystalline order. These structural advantages contribute to a higher fill factor (FF) and short-circuit current density (J_{SC}) in D18/Py7 devices. Regarding the V_{OC}, consistent with our previous report, the chlorinated acceptor Py7 achieves a significantly higher V_{OC}, which is closely linked to its minimized non-radiative recombination of 0.267 eV. Theoretical simulations reveal that in the triplet state, the hole and electron densities partially overlap in the central Qx ring of Py7, leading to smaller energy difference between the lowest triplet charge-transfer state and the lowest singlet state, which may be conducive to promoting triplet-to-singlet conversion and suppressing non-radiative recombination losses. Further studies reveal that introducing Cl decreases the charge transfer state ratio of D18/acceptor. These concurrent enhancements in J_{SC}, FF and V_{OC} result in a better PCE of 18.51% for Py7-based device. Moreover, through the mutual dilution strategy of donor and acceptor, the (D18:1wt% Py7)/(Py7:1wt% D18) device yields an impressive PCE of 19.60%, representing the best performance achieved in binary OSCs that do not incorporate BTA-core-based acceptors. Our work not only highlights the significant photovoltaic potential of the Py-series acceptors but also shows that chlorination can improve molecular packing while simultaneously reducing non-radiative energy losses.

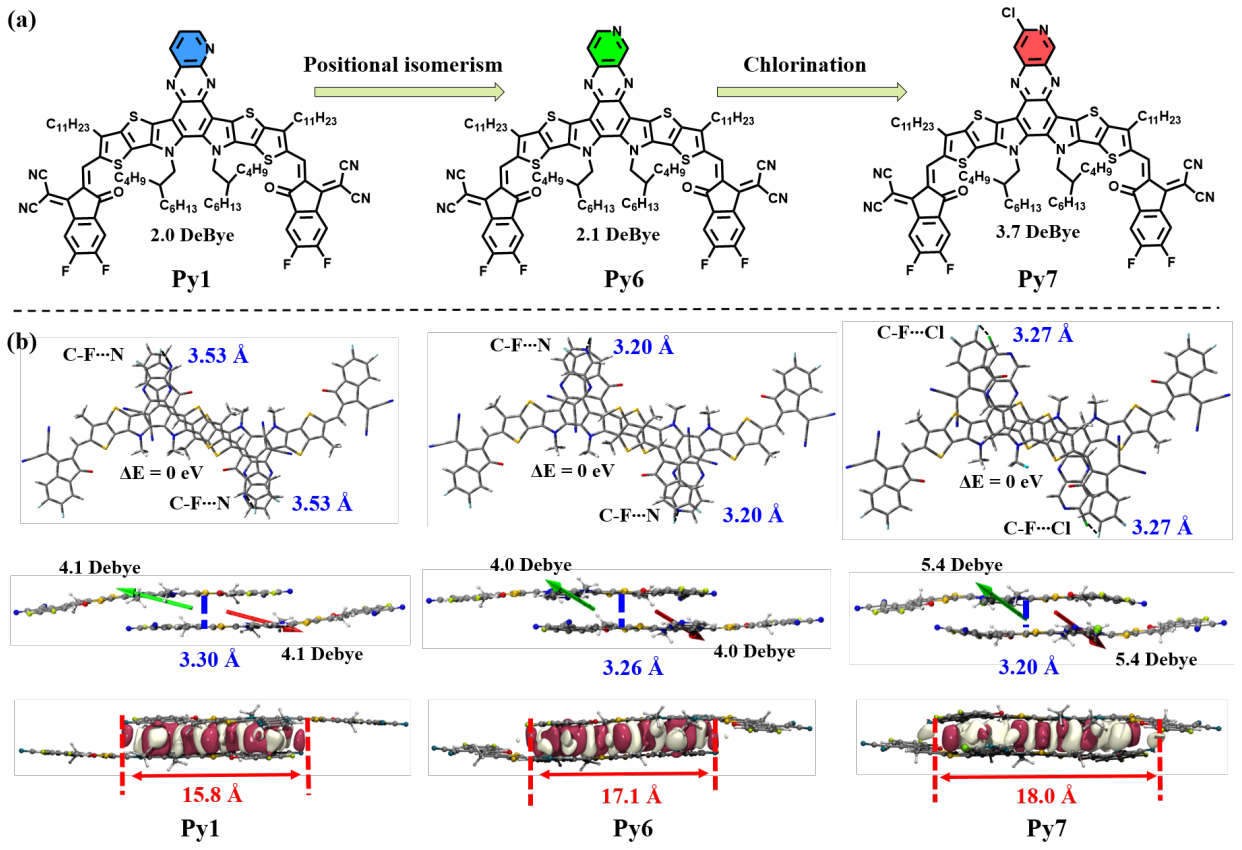

Figure 1. (a) Molecular structures of Py1, Py6 and Py7; (b) The optimal dimer for Py1, Py6 and Py7.

Results and discussion

The chemical structures of three acceptors, Py1, Py6 and Py7, are displayed in **Figure 1a**, and the synthetic procedures for Py6 and Py7 are provided in Scheme S1-S4 in the surpporting information, and can be referenced from our previous report.[27] These SMAs exhibit excellent solubility in various commonly used solvents, including chloroform (CF), chlorobenzene (CB), toluene (Tol), tetrahydrofuran (THF), *o*-xylene (*o*-XY).

To examine the effects of nitrogen positional isomerism in pyridine and chlorination on the physicochemical properties of SMAs, we first conducted DFT calculations to analyze the single-molecule dipole moments and molecular geometries. As summarized in Table 1, Py1 and Py6 display comparable single-molecule dipole moments (2.0 Debye and 2.1 Debye, respectively), while the introduction of chlorine atoms notably increases the dipole moment, as seen in Py7 (3.7 Debye). As depicted in Figure S1, all three SMAs maintain good molecular planarity, with similar N-C-C-N dihedral angles of approximately 9.5°.

To further delve into the intermolecular interactions, we optimized the four dimer conformations of the three PyQx-series acceptors. As illustrated in Figures S2-S4, these acceptors exhibit two primary stacking modes: IC/IC packing and IC/PyQx packing. Based on the steady-state energy of the different dimers, we selected the dimer with the lowest energy for representation in **Figure 1b**. The relative energy is the difference in single-point energy between each dimer and the dimer with the lowest energy.[51] It was observed that the optimal dimers of all three acceptors predominantly adopt the IC/PyQx stacking mode. Compared with Py1, the positional isomerism of the N atom in Py6 results in a shorter C-F···N distance (3.53 Å for Py1 *vs* 3.20 Å for Py6). In contrast to Py1 and Py6, Py7 does not exhibit the C-F···N interaction but instead features a strong C-F···Cl interaction. Examining the dipoles of the monomers within the dimers, Py1 and Py6 show similar dipole moments (around 4.0 Debye), while the addition of chlorine in Py7 increases the dimer's monomer dipoles, consistent with the trend in single-molecule dipole moments. Due to the strong dipole-dipole interaction and tight intermolecular non-covalent bonding, Py7 exhibits the smallest π-π stacking distance of 3.20 Å and the largest LUMO overlap length of 18.0 Å relative to those of Py1 and Py6 (π-π stacking distance: 3.30 Å for Py1 and 3.26 Å for Py6; LUMO overlap length: 15.8 Å for Py1 and 17.1 Å for Py6).

Table 1. Optical and electrochemical data of Py1, Py6, and Py7.

Acceptor	λ_{max}^{sol} (nm)	λ_{max}^{film} (nm)	λ_{onset}^{film} (nm)	E_g^{opt} (eV)	LUMO[b] (eV)	HOMO[b] (eV)	LUMO[c] (eV)	HOMO[c] (eV)	E_g^{DFT} (eV)	Dipole moments (Debye)
Py1	738	835	943	1.31	−4.00	−5.72	−3.71	−5.73	2.02	2.0
Py6	733	822	926	1.34	−4.01	−5.74	−3.76	−5.79	2.03	2.1
Py7	730	814	914	1.36	−4.03	−5.77	−3.79	−5.84	2.05	3.7

[a]Calculated from $E_g^{opt} = 1240/\lambda_{onset}$; [b]Calculated from CV curves; [c]Obtained from DFT calculations.

Grazing-incidence wide-angle X-ray scattering (GIWAXS) was performed to analyze the crystalline behaviors of the three neat acceptor films, with 2D GIWAXS patterns and the corresponding in-plane (IP) and out-of-plane (OOP) line-cut profiles shown in **Figure 2a** and **2b**. All three acceptors predominantly exhibit a face-on orientation, characterized by distinct π-π stacking (010) diffraction peaks in the OOP direction, which facilitates efficient vertical charge transport. In detail, Py7 exhibits a shorter π-π stacking distance (*d*-spacing) of 3.54 Å and an enhanced crystalline coherence length (CL) of 17.93 Å, as compared with Py1 (*d*-spacing: 3.56 Å; CL: 17.36 Å) and Py6 (*d*-spacing: 3.72 Å; CL: 17.48 Å). In the IP direction, the highest diffraction intensity and largest CL of 59.32 Å were observed for Py7. These findings imply that Py7 demonstrates better crystallite ordering and the tightest molecular stacking, benefiting the electron transport. Consequently, Py7 achieves an electron mobility (μ_e) of up to 9.28 × 10^{-4} cm^2 V^{-1} s^{-1}, as measured by the space charge limited current (SCLC) method, outperforming Py1 (4.56 × 10^{-4} cm^2 V^{-1} s^{-1}) and Py6 (5.67 × 10^{-4} cm^2 V^{-1} s^{-1}), which coincides with the GIWAXS results.

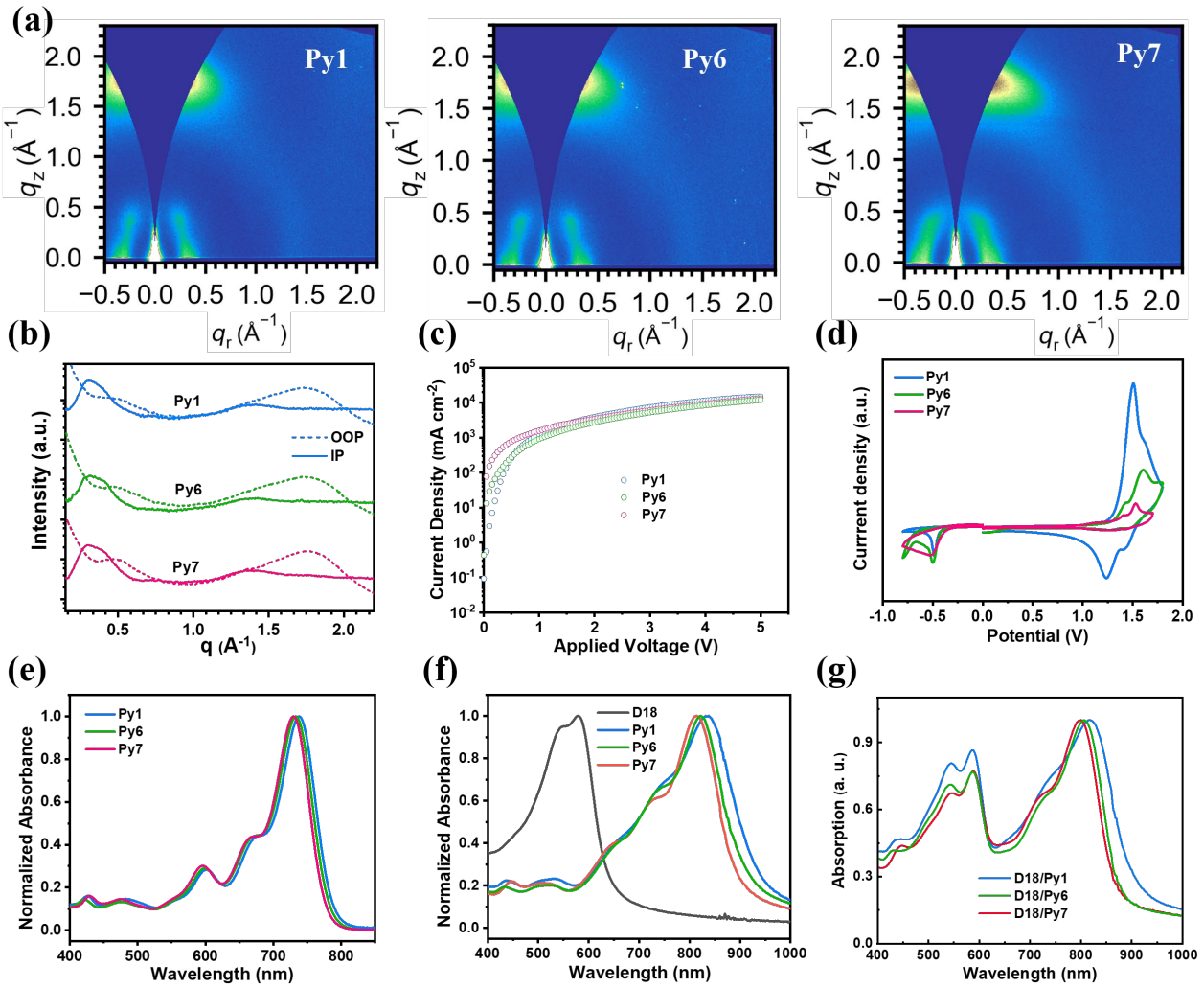

Figure 2. (a) 2D GIWAXS patterns and (b) the in-plane and out-of-plane line-cut profiles of Py1, Py6 and Py7 neat films; (c) *J*-*V* characteristics in dark for electron-only devices based on Py1, Py6 and Py7; (d) CV curves of Py1, Py6 and Py7 in thin films; (e) Normalized absorption spectra of Py1, Py6 and Py7 in CF solution; (f) Normalized absorption spectra of Py1, Py6, Py7 and D18; (g) Normalized absorption spectra of D18/Py1, D18/Py6 and D18/Py7 blend films.

Cyclic voltammetry (CV) measurements were conducted to determine the LUMO energy level (E_{LUMO}) and HOMO energy level (E_{HOMO}) of these three PyQx-series acceptors. As presented in **Figure 2d**, all the acceptors display obvious reduction and oxidation potentials, the onset reduction/oxidation potentials of Py1, Py6, and Py7 *versus* Ag/Ag^+ were recorded as −0.41 eV/1.31 eV, −0.40 eV/1.33 eV, and −0.38 eV/1.36 eV, respectively, with the Fc/Fc^+ energy level at 0.39 eV and an assumed vacuum level of −4.8 eV. Therefore, the E_{LUMO}/E_{HOMO} values are estimated to be −4.00/−5.72 eV for Py1, −4.01/−5.74 eV for Py6, and −4.03/−5.77 eV for Py7, respectively, which align with the trends observed in the DFT calculations. Furthermore, we employed ultraviolet-visible (UV−Vis) spectroscopy to ascertain the absorption features of the three SMAs in CF solution and thin film (**Figure 2e-g**). In CF solution, the maximum absorption peaks for Py1, Py6 and Py7 are 738, 733 and 730 nm, respectively. This trend suggests that the positional change of the nitrogen atom and chlorination weakens the electron-donating ability of the central core, leading to a reduced intramolecular charge transfer (ICT) effect (**Figure 2e**). Upon transitioning from solution to film, all three acceptors exhibit a noticeable red shift in absorption, attributed to the intermolecular stacking effect in the solid state. Interestingly, the gradual suppression of the 0-1 peak from Py1 to Py6 and then to Py7 indicates increasingly pronounced J-aggregation in the order of Py1, Py6, and Py7 (**Figure 2f**).[52, 53] A similar phenomena is observed in the absorption spectra of the D18/SMA blend films (**Figure 2g**). In addition, the D/A blend films demonstrate a wide absorption range from 400 to 910 nm, contributing to a high J_{SC}.

Table 2. Device data of D18/acceptors-based devices. Values in parentheses are averages based on at least 10 independent devices.

Devices	V_{OC} (V)	J_{SC} (mA cm^{-2})	FF %	PCE %
Py1	0.764	22.46	62.4	10.71 (10.35 ± 0.29)
Py6	0.723	26.07	69.0	13.01 (12.67 ± 0.25)
Py7	0.877	26.78	78.8	18.51 (18.28 ± 0.22)
Py7[a]	0.885	27.72	79.9	19.60 (19.18 ± 0.37)

[a]: The optimal (D18:1wt% Py7)/(Py7:1wt% D18) device.

To explore the photovoltaic potential of three PyQx-based acceptors, we prepared photovoltaic cells using a conventional structure of ITO/PEDOT/D18/acceptors/PFN-Br/Ag. The detailed device

fabrication process is outlined in the Supplementary Information (SI). **Figure 3a** illustrates the current density−voltage (*J*−*V*) curves of the optimal device, with the related photovoltaic parameters provided in **Table 2**.

Basically, the D18/Py1 device realizes a relatively low efficiency of 10.71%, primarily ascribed to the three poor basic PV parameters (open-circuit voltage (V_{OC}) = 0.764 V; J_{SC} = 22.46 mA cm^{-2}; FF = 0.690). When the nitrogen atom position on the pyridine ring in Py1 is altered, the D18/Py6-based device achieves a higher J_{SC} (26.07 mA cm^{-2}) and FF (0.690), leading to an improved device efficiency (13.01%), which is closely associated with the better morphology of its blended film. With the chlorination of Py6, the Py7-based device attains a significantly higher V_{OC} (0.877 V) and FF (0.788), resulting in the highest PCE of 18.51%. It is worth noting that the V_{OC} of Py7-based device is 0.15 V higher than that of Py6-based device, which is closely related to its lower energy loss (as discussed below). **Figure 3b** presents the external quantum efficiency (EQE) curves of D18/SMA devices. It can be clearly observed that D18/Py7 device exhibits a higher EQE response across the 400–855 nm wavelength range, as compared with D18/Py1 and D18/Py6 device. The integrated J_{SC} values are 21.62, 25.36, and 25.93 mA cm^{-2} for D18/Py1, D18/Py6, and D18/Py7 devices, respectively, confirming the reliability of cell efficiency. To assess the stability of the device, we examined the variations in performance parameters of unpackaged devices. As shown in Figure S5, after 2 hours of UV irradiation (365 nm), with a focus on Py1 and Py6, we observed that the isomerization strategy (from Py1 to Py6) resulted in a more substantial degradation in V_{OC} and FF. However, upon chlorinating Py6, the loss in V_{OC} and FF was significantly suppressed, suggesting that the incorporation of chlorine improved the device stability.

To assess the charge recombination and extraction characteristics of D18/SMA devices, we carried out the transient photovoltage (TPV) and transient photocurrent (TPC) tests, as shown in **Figure 3c** and Figure S6. The TPV curves reveal carrier lifetimes of 0.81 μs for the D18/Py1 device, 1.65 μs for the D18/Py6 device, and 3.54 μs for the D18/Py7 device, respectively, indicating that Py7-based device experiences the least charge recombination. The charge sweep-out times from the TPC curves are 0.16, 0.14, and 0.12 μs for the D18/Py1, D18/Py6, and D18/Py7 devices, respectively, suggesting the best charge extraction ability in Py7-based device. The longest carrier lifetimes and the fastest TPC decay may be an important reason for the highest FF observed in D18/Py7 device.

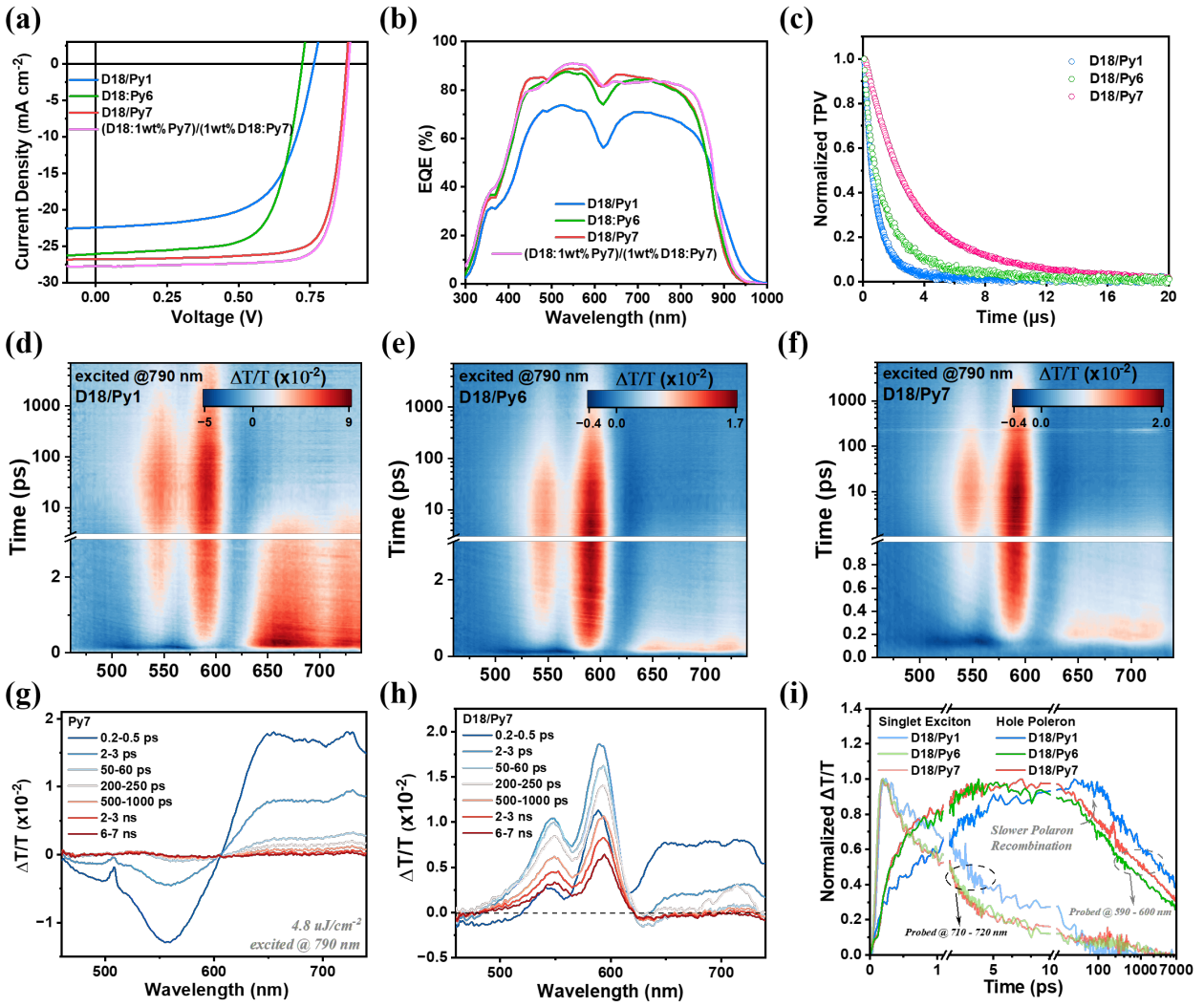

Figure 3. (a) *J–V* curves and (b) EQE curves of the optimal devices based on D18/Py1, D18/Py6, D18/Py7, and (D18+1wt%Py7)/(Py7+1wt%D18); (c) TPV results after normalization for D18/Py1, D18/Py6, D18/Py7 device; (d-f) 2D contour maps of TAS measurements on D18/SMA blend films. Time scale spectral lines of TAS results for (g) Py7 neat film and (h) D18/Py7 blend; (i) The extracted singleton and polaron kinetics for D18/Py1, D18/Py6, D18/Py7 device.

To more comprehensively demonstrate charge behaviors, the femto-second transient absorption spectroscopy (fs-TAS) measurement is applied to neat and blend films, with the results presented in 2D contour maps (**Figure 3d-f** and Figure S7), representative time spectra (**Figure 3g**, **3h**, and Figure S8), and extracted exciton kinetics (**Figure 3i**). The excited laser wavelength is chosen as 790 nm, while the detection and analysis are carried out at the visible light region. Accordingly, acceptor films uniformly possess significant photobleaching (PB) signals at > 700 nm range, thus the signals of blend films extracted from 710 to 720 nm can be taken as the tracker of excited singlet excitons. On the other hand, neat acceptor films demonstrate very weak excited absorption (EA) signals at 600 nm, which are all covered by the PB signals of D18 in blend films. Thereby, the time dependent intensity here can represent the generation and recombination kinetics of hole polaron, that are acknowledged

as a precise mark of the process of exciton dissociation and free carrier recombination.[54-56] Thus, we can clearly figure out that the hole transfer speed and charge generation efficiency is significantly enhanced by isomerization strategy, though its polaron decay kinetics is the slowest. Specifically, for Py1-, Py6-, and Py7-based blends, the charge generation times are as follows: for Py1, $\tau_1 = 0.64$ ps and $\tau_2 = 5.05$ ps; for Py6, $\tau_1 = 0.35$ ps and $\tau_2 = 1.59$ ps and for Py7, $\tau_1 = 0.36$ ps and $\tau_2 = 1.35$ ps. The Py1 based blend possesses much slower charge generation speed than another two blends. Regarding charge dissociation times (or decay lifetimes), the values are: for Py1, $\tau_1 = 118$ ps and $\tau_2 = 2070$ ps; for Py6, $\tau_1 = 91$ ps and $\tau_2 = 1319$ ps and for Py7, $\tau_1 = 107$ ps and $\tau_2 = 1179$ ps. The Py7-based blend demonstrates a longer charge dissociation lifetime than the Py6-based blend, resulting in a lower rate of bimolecular recombination and contributing to higher FF. D18/Py7 demonstrates both favorable charge generation process and slowed free carrier recombination process, consistent with the TPC/TPV results.

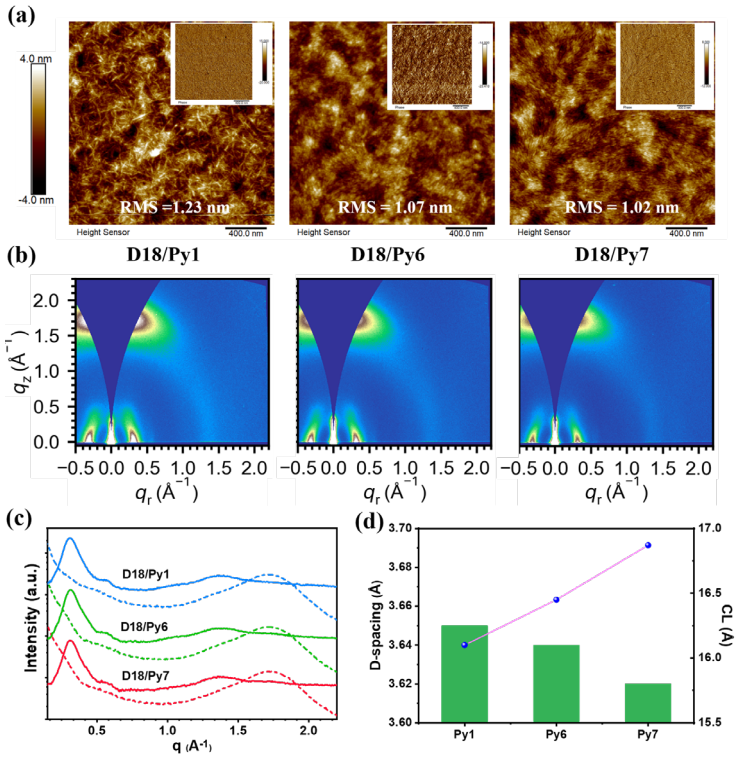

Figure 4. (a) AFM height images and AFM phase images of D18/Py1, D18/Py6, D18/Py7 blend films; (b) 2D GIWAXS patterns and (c) in-plane and out-of-plane line-cut profiles from 2D GIWAXS data of the D18/Py1, D18/Py6, D18/Py7 blend films; (d) Crystalline parameters of π–π stacking distance and coherence length for D18/Py1, D18/Py6, D18/Py7 blend films in the OOP direction.

To gain a better understanding of how blend film morphology affects device performance, we utilized atomic force microscopy (AFM) and GIWAXS technology to thoroughly probe the surface morphology, molecular stacking and crystallization characteristics the active layers. **Figure 4a** presents AFM height images with smooth surface structures across all three blends, where the root

mean-square roughness (RMS) values are closely comparable: Py1 at 1.23 nm, Py6 at 1.07 nm, and Py7 at 1.02 nm. The similar AFM phase images indicate that surface morphology of the blend films does not play a significant role in determining device performance.

Focusing on the GIWAXS results (**Figure 4b-d**), the blend films of D18/Py1, D18/Py6, and D18/Py7 primarily demonstrate a face-on orientation, with a pronounced 010 diffraction peak (D18/Py1: $q_z \sim 1.720$ Å; D18/Py6: $q_z \sim 1.720$ Å; D18/Py7: $q_z \sim 1.720$ Å) in the OOP direction. Specifically, D18/Py7 features a smaller *d*-spacing of 3.62 Å and a greater CL of 16.87 Å, compared to those of blends based on D18/Py1 (*d*-spacing: 3.64 Å; CL: 16.10 Å) and D18/Py6 (d-spacing: 3.64 Å; CL: 16.45 Å), indicating more compact molecular packing and improved crystalline order of D18/Py7 blend. A similar trend is observed in the IP direction. The GIWAXS results show that both isomerization and chlorination contribute to a reduction in intermolecular stacking distance and an enhancement in crystal order. To evaluate charge-transport features, we applied SCLC technology to measure the hole mobility (μ_h) and μ_e for D18/acceptors blends (Figure S9). The recorded μ_e/μ_h values were 3.86/6.36, 5.29/7.15, and 8.92/8.78 × 10^{-4} cm^2 V^{-1} s^{-1} for D18/Py1, D18/Py6, and D18/Py7, with corresponding μ_e/μ_h ratios of 0.61, 0.74, and 1.03, respectively. The excellent charge transport properties are crucial for the superior FF observed in the Py7-based device.

Apart from the favorable active-layer morphology, another key factor contributing to the superior efficiency of the D18/Py7 device is its significantly higher V_{OC}. To understand the underlying mechanism behind high V_{OC}, we performed Fourier transform photocurrent spectroscopy (FTPS)-EQE and electroluminescence (EL) test. As indicated in **Figure 5a** and **5b**, the D18/Py7 device shows the lowest energy loss (E_{loss}) of 0.554 eV compared to 0.598 eV for D18/Py1 and 0.695 eV for D18/Py6, which is primarily attributed to its smaller non-radiative losses of 0.267 eV (Table S1). To further investigate the variation in non-radiative energy losses, we first conducted time-dependent (TD)-DFT calculations on the lowest singlet (S_1) excited states in the optimal D18:PyX blend systems, finding that electron density primarily concentrates on PyX, with some hole density extending to D18 (Figure S10), which signifies a mixture of charge transfer (CT) and local excitation (LE) states. Notably, when a higher proportion of CT states is present, it can lead to increased recombination losses due to non-radiative decay pathways. The CT ratios are 25.6% for Py1, 31.6 for Py6, and 23.8% for Py7 (**Figure 5c**), respectively, indicating a diminished contribution of charge transfer character following chlorination, which coincides with the EQE_{EL} results.[57, 58] Additionally, we performd TD-DFT calculations for the singlet and triplet excited states of three acceptor molecules (Figure S11). We found that both S_1 and the lowest triplet (T_1) excited states are characterized predominantly by LE features, suggesting that direct triplet-to-singlet conversion between S_1 ($^1LE_1$) and T_1 ($^3LE^1$) is likely very inefficient.[59, 60] Consequently, we focused on the

intermediate higher-lying triplet states that exhibit charge-transfer characteristics. Notably, our calculations showed that Py7 exhibited the lowest triplet charge-transfer excited state ($^3CT_1$) energy of 1.840 eV, which is lower than those of Py1 (1.924 eV) and Py6 (1.901 eV).

To elucidate the changes in the excited state properties of $^3CT_1$, we analyzed the distribution of hole and electron natural transition orbitals in the three SMAs. In Py1 and Py6, the electron density is primarily localized in the PyQx unit, while the hole density is concentrated in the central thiophene unit (**Figure 5d**), indicating that the CT state forms on the triplet state ($^3CT_1$). Interestingly, in Py7, the introduction of Cl causes the hole density to diffuse toward the central PyQx unit. This suggests the formation of a hybrid local-CT excited state ($^3HLCT_1$), where the hole and electron densities partially overlap on the central Qx ring. Consequently, Py7 exhibits a very small energy difference between $^3CT_1$ and $^1LE_1$—approximately 0.004 eV. This minimal difference facilitates the triplet-to-singlet conversion process, helping to reduce the non-radiative energy loss associated with the triplet state.[61, 62]

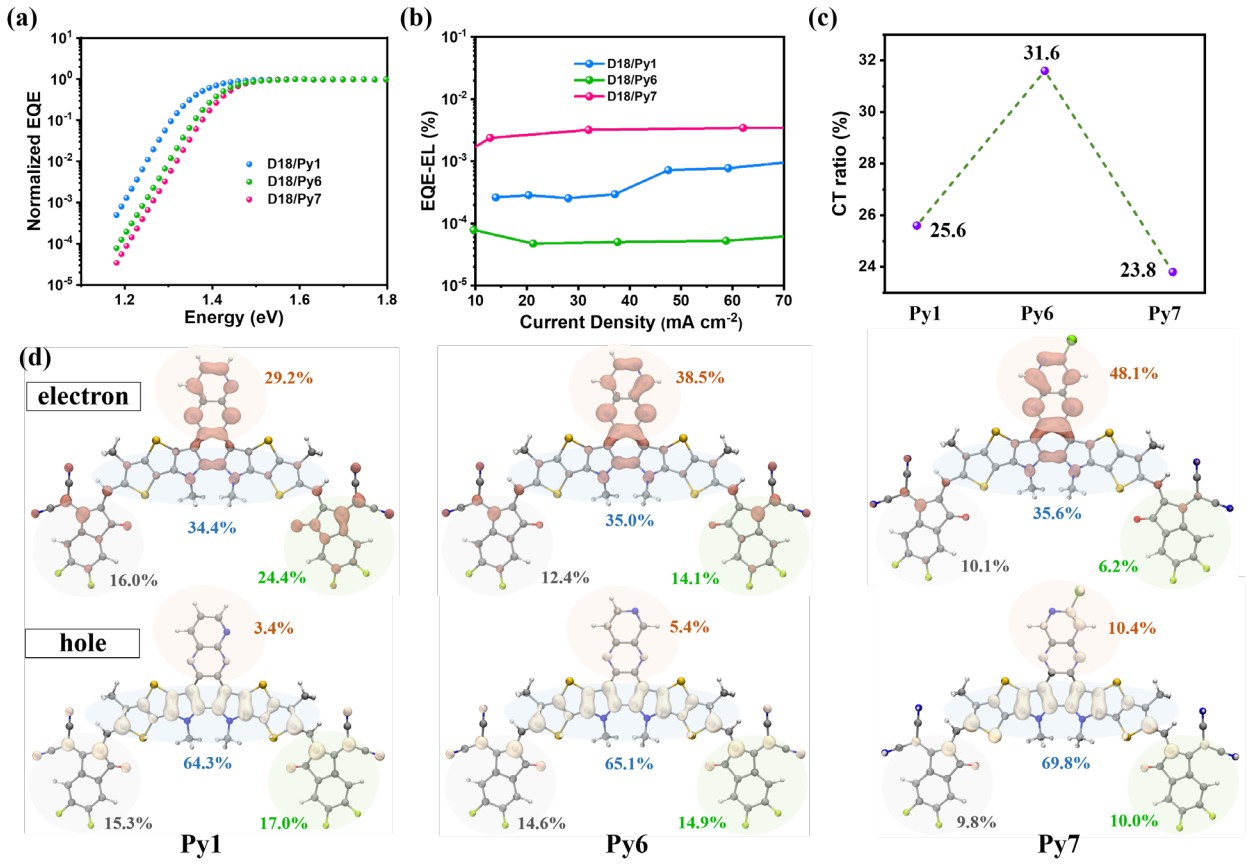

Figure 5. (a) FTPS-EQE spectra and (b) EQE_{EL} results for D18/Py1, D18/Py6, D18/Py7 device; (c) CT ratio in the three blend systems; (d) Calculated fractions of holes and electrons for Py1, Py6 and Py7.

To further explore the photovoltaic potential of Py7, we used a donor-acceptor mutual dilution

strategy, wherein 1% of the acceptor by mass was added to the donor phase and 1% of the donor by mass was added to the acceptor phase for layer-by-layer deposition to construct devices (**Figure 3a**). Remarkably, the (D18:1wt% Py7)/ (Py7:1wt% D18) device yielded an excellent PCE of 19.60%, along with a high FF of 0.799 and a good J_{SC} of 27.72 mA cm^{-2}. The high J_{SC} is further supported by the EQE curves shown in **Figure 3b**. As far as we know, the PCE of 19.60% ranks among the highest reported for binary OSCs utilizing A-DA$_1$D-A-type acceptors with novel electron-deficient units distinct from benzothiadiazole. Additionally, we employed the donor-acceptor mutual dilution strategy with Py1 and Py6 to assess the broader applicability of this approach. As shown in Figure S12 and Table S2, the device performance of the (D18:1wt% Py1)/(Py1:1wt% D18) device and the (D18:1wt% Py6)/(Py6:1wt% D18) device was enhanced by this strategy, compared to their respective D18/acceptor devices, demonstrating the generality of the approach. Notably, the overall trend remained consistent with that observed for the different D18/acceptor devices.

Conclusion

In summary, we introduced two new SMAs (Py6 and Py7), building upon our earlier progress in developing the Py-series of photovoltaic acceptors. Compared to Py1, the positional isomerism of the N atom on pyridine ring gives Py6 a larger crystalline coherence length, leading to improved electron mobility. Furthermore, the chlorination of Py6 endows Py7 with tighter molecular packing and better crystalline order, as validated by theoretical calculations and GIWAXS data. As a result, the D18/Py7 device reaches an enhanced PCE of 18.51%, as compared with D18/Py1 (10.71%) and D18/Py6 (13.01%) devices, attributed to the better charge transport/extraction ability, more favorable morphology and minimized nonradiative energy loss. Further studies demonstrate that introduction of Cl directs the hole density toward the central PyQx unit and decreases the charge transfer state ratio of D18/acceptor. This promotes triplet-to-singlet conversion process and suppresses triplet state-related non-radiative recombination losses. Moreover, by employing a mutual dilution strategy of donor and acceptor, the (D18:1wt% Py7)/(Py7:1wt% D18) device delivers a remarkable PCE of 19.60%. Our study not only underscores the strong photovoltaic potential of the Py-series acceptors, but more importantly, uncovers the underlying mechanism by which chlorination reduces non-radiative energy losses.

Data Availability Statement

The data that support the findings of this study are available from the corresponding author upon reasonable request.

Conflicts of interest

Authors declare no conflicts of interest.

Acknowledgements

H. Tian, Y. Luo, Z. Chen contributed equally to this work. Z. Luo thanks the National Natural Science Foundation of China (NSFC, Nos. 22475133, and 22309119), and the Shenzhen Science and Technology Program (Nos. 20231120182602001, RCBS20221008093225021). G. Li acknowledges the support from Research Grants Council of Hong Kong (Project Nos. 15221320, 15307922, C7018-20G, C5037-18G, C4005-22Y), RGC Senior Research Fellowship Scheme (SRFS2223-5S01). R. Ma thanks the PolyU Distinguished Postdoctoral Fellowship (1-YW4C). J. Wu thanks the Guangzhou government for funding (2021QN02C110), the Guangzhou Municipal Science and Technology Project (No. 2023A03J0097, No. 2023A03J0003, 2024A04J4513No. 2023A03J0097 and No. 2023A03J0003), and NSFC (52303249). We also thank the Instrumental Analysis Center of Shenzhen University for the analytical support and the Green Materials Laboratory and the Materials Characterization and Preparation Facility (MCPF) at the Hong Kong University of Science and Technology (Guangzhou) for their facilities and technical support.

[1] L. Ye, H. Hu, M. Ghasemi, T. Wang, B. A. Collins, J. −H. Kim, K. Jiang, J. H. Carpenter, H. Li, Z. Li, T. McAfee, J. Zhao, X. Chen, J. L. Y. Lai, T. Ma, J. −L. Bredas, H. Yan, H. Ade, *Nat. Mater.* **2018**, *17*, 253

[2] G. Zhang, F. R. Lin, F. Qi, T. Heumüller, A. Distler, H. -J. Egelhaaf, N. Li, P. C. Y. Chow, C. J. Brabec, A. K.-Y. Jen, H. –L. Yip, *Chem. Rev.* **2022**, *122*, 14180.

[3] W. Gao, M. Jiang, Z. Wu, B. Fan, W. Jiang, N. Cai, H. Xie, F. R. Lin, J. Luo, Q. An, H. Y. Woo, A. K. Y. Jen. *Angew. Chem. Int. Ed.* **2022**, *61*, e202205168.

[4] W. Wei, R. Ma, Z. Chen, T. Xu, G. Li, Z. Luo, *Chin. J. Chem.* **2024**, *42,* 623.

[5] W. Zhang, Y. Wu, R. Ma, H. Fan, X. Li, H. Yang, C. Cui, Y. Li, *Angew. Chem. Int. Ed.* **2023**, *62*, e2023097.

[6] K. Chong, X. Xu, H. Meng, J. Xue, L. Yu, W. Ma, Q. Peng, *Adv. Mater.* **2022**, *34*, 2109516.

[7] G. Li, V. Shrotriya, J. Huang, Y. Yao, T. Moriarty, K. Emery, Y. Yang, *Nat. Mater.* **2005**, *4*, 864.

[8] Y. Liu, B. Liu, C. −Q. Ma, F. Huang, G. Feng, H. Chen, J. Hou, L. Yan, Q. Wei, Q. Luo, Q. Bao, W. Ma, W. Liu, W. Li, X. Wan, X. Hu, Y. Han, Y. Li, Y. Zhou, Y. Zou, Y. Chen, Y. Li, Y. Chen, Z. Tang, Z. Hu, Z. −G. Zhang, Z. Bo, *Sci. China Chem.* **2021**, *65*, 224.

[9] J. Fu, Q. Yang, P. Huang, S. Chung, K. Cho, Z. Kan, H. Liu, X. Lu, Y. Lang, H. Lai, F. He, P. W. K. Fong, S. Lu, Y. Yang, Z. Xiao, G. Li, *Nat. Commun.* **2024**, *15*, 1830.

[10] J. Fu, P. W. K. Fong, H. Liu, C. −S. Huang, X. Lu, S. Lu, M. Abdelsamie, T. Kodalle, C. M. Sutter-Fella, Y. Yang, G. Li, *Nat. Commun.* **2023**, *14*, 1760.

[11] F. Yi, M. Xiao, Y. Meng, H. Bai, W. Su, W. Gao, Z. F. Yao, G. Qi, Z. Liang, C. Jin, L. Tang, R. Zhang, L. Yan, Y. Liu, W. Zhu, W. Ma, Q. Fan, *Angew. Chem. Int. Ed.* **2024**, *63*, e202319295.

[12] J. Hou, O. Inganas, R. H. Friend, F. Gao, *Nat. Mater.* **2018**, *17*, 119.

[13] C. Yan, J. Qin, Y. Wang, G. Li, P. Cheng, *Adv. Energy Mater*. **2022**, 12, 2201087.

[14] B. Zou, W. Wu, T. A. Dela Peña, R. Ma, Y. Luo, Y. Hai, X. Xie, M. Li, Z. Luo, J. Wu, C. Yang, G. Li, H. Yan, *Nano-Micro Letters* **2023**, *16*, 30.

[15] B. Liu, W. Xu, R. Ma, J. −W. Lee, T. A. Dela Peña, W. Yang, B. Li, M. Li, J. Wu, Y. Wang, C. Zhang, J. Yang, J. Wang, S. Ning, Z. Wang, J. Li, H. Wang, G. Li, B. J. Kim, L. Niu, X. Guo, H. Sun, *Adv. Mater.* **2023**, *35*, 2308334.

[16] J. Fu, P. W. K. Fong, H. Liu, C. S. Huang, X. Lu, S. Lu, M. Abdelsamie, T. Kodalle, C. M. Sutter-Fella, Y. Yang, G. Li, *Nat. Commun.* **2023**, *14*, 1760.

[17] J. Wang, P. Xue, Y. Jiang, Y. Huo, X. Zhan, *Nat. Rev. Chem.* **2022**, *6*, 614.

[18] Y. Ma, M. Zhang, S. Wan, P. Yin, P. Wang, D. Cai, F. Liu, Q. Zheng, *Joule*, **2021**, *5*, 197.

[19] Y. Wei, Z. Chen, G. Lu, N. Yu, C. Li, J. Gao, X. Gu, X. Hao, G. Lu, Z. Tang, J. Zhang, Z. Wei, X. Zhang, H. Huang, *Adv. Mater.* **2022**, *34*, 2204718.

[20] S. Liang, C. Xiao, C. Xie, B. Liu, H. Fang, W. Li, *Adv. Mater.* **2023**, *35*, 2300629.

[21] T. Lin, Y. Hai, Y. Luo, L. Feng, T. Jia, J. Wu, R. Ma, T. A. Dela Pena, Y. Li, Z. Xing, M. Li, M. Wang, B. Xiao, K. S. Wong, S. Liu, G. Li, *Adv. Mater.* **2024**, *36*, 2312311.

[22] J. Wu, Z. Ling, L. R. Franco, S. Y. Jeong, Z. Genene, J. Mena, S. Chen, C. Chen, C. M. Araujo, C. F. N. Marchiori, J. Kimpel, X. Chang, F. H. Isikgor, Q. Chen, H. Faber, Y. Han, F. Laquai, M. Zhang, H. Y. Woo, D. Yu, T. D. Anthopoulos, E. Wang, *Angew. Chem. Int. Ed.* **2023**, 62, e202302888.

[23] C. Li, J. Zhou, J. Song, J. Xu, H. Zhang, X. Zhang, J. Guo, L. Zhu, D. Wei, G. Han, J. Min, Y. Zhang, Z. Xie, Y. Yi, H. Yan, F. Gao, F. Liu, Y. Sun, *Nat. Energy* **2021**, *6*, 605.

[24] H. Lai, H. Chen, Z. -Y. Chen, Y. Lang, Y. Zhu, S. −T. Zhang, X. Lai, P. Tan, Y. Zhang, B. Yang, G. Li, F. He, *Energy Environ. Sci.* **2023**, *16*, 5944.

[25] R. Zeng, M. Zhang, X. Wang, L. Zhu, B. Hao, W. Zhong, G. Zhou, J. Deng, S. Tan, J. Zhuang, F. Han, A. Zhang, Z. Zhou, X. Xue, S. Xu, J. Xu, Y. Liu, H. Lu, X. Wu, C. Wang, Z. Fink, T. P. Russell, H. Jing, Y. Zhang, Z. Bo, F. Liu, *Nat. Energy* **2024**, https://doi.org/10.1038/s41560-024-01564-0.

[26] C. He, Y. Pan, Y. Ouyang, Q. Shen, Y. Gao, K. Yan, J. Fang, Y. Chen, C.-Q. Ma, J. Min, C. Zhang, L. Zuo, H. Chen, *Energy Environ. Sci.* **2022**, *15*, 2537

[27] T. Xu, Z. Luo, R. Ma, Z. Chen, T. A. Dela Pena, H. Liu, Q. Wei, M. Li, C. Zhang, J. Wu, X. Lu, G. Li, C. Yang, *Angew. Chem. Int. Ed.* **2023**, *62*, e202304127.

[28] R. Ma, C. Yan, P. W.-K. Fong, J. Yu, H. Liu, J. Yin, J. Huang, X. Lu, H. Yan, G. Li, *Energy Environ. Sci*. **2022**, 15, 2479.

[29] J. Yuan, Y. Zhang, L. Zhou, G. Zhang, H.-L. Yip, T.-K. Lau, X. Lu, C. Zhu, H. Peng, P. A. Johnson, Y. Li, Y. Zou, *Joule* **2019**, *3*, 1140.

[30] Y. Lin, J. Wang, Z. −G. Zhang, H. Bai, Y. Li, D. Zhu, X. Zhan, *Adv. Mater.* **2015**, *27*, 1170.

[31] X. Zhao, Q. An, H. Zhang, C. Yang, A. Mahmood, M. Jiang, M. H. Jee, B. Fu, S. Tian, H. Y. Woo, Y. Wang, J. Wang, *Angew. Chem. Int. Ed.* **2023**, *62*, e2216340.

[32] Y. Cui, P. Zhu, H. Hu, X. Xia, X. Lu, S. Yu, H. Tempeld, R.-A. Eichel, X. Liao, Y. Chen, *Angew. Chem. Int. Ed.* **2023**, 62, e202304931.

[33] S. Guan, Y. Li, C. Xu, N. Yin, C. Xu, C. Wang, M. Wang, Y. Xu, Q. Chen, D. Wang, L. Zuo, H.

Chen, *Adv. Mater.* **2024**, *36*, e2400342.

[34] Y. Sun, L. Wang, C. Guo, J. Xiao, C. Liu, C. Chen, W. Xia, Z. Gan, J. Cheng, J. Zhou, Z. Chen, J. Zhou, D. Liu, T. Wang, W. Li, *J. Am. Chem. Soc.* **2024**,*146*, 12011.

[35] Z. Chen, J. Ge, W. Song, X. Tong, H. Liu, X. Yu, J. Li, J. Shi, L. Xie, C. Han, Q. Liu, Z. Ge, *Adv. Mater.* **2024**, *36*, 2406690.

[36] L. Zhu, M. Zhang, G. Zhou, Z. Wang, W. Zhong, J. Zhuang, Z. Zhou, X. Gao, L. Kan, B. Hao, F. Han, R. Zeng, X. Xue, S. Xu, H. Jing, B. Xiao, H. Zhu, Y. Zhang, F. Liu, *Joule* **2024**, https://doi.org/10.1016/j.joule.2024.08.001.

[37] C. Chen, L. Wang, W. Xia, K. Qiu, C. Guo, Z. Gan, J. Zhou, Y. Sun, D. Liu, W. Li, T. Wang, *Nat. Commun.* **2024**, *15*, 6865.

[38] Y. Jiang, S. Sun, R. Xu, F. Liu, X. Miao, G. Ran, K. Liu, Y. Yi, W. Zhang, X. Zhu, *Nat. Energy* **2024**, *9*, 975.

[39] K. Liu, Y. Jiang, F. Liu, X. Zhu, *Energy Environ. Sci.* **2024**, *17*, 4944.

[40] M. Xie, Z. Wei, K. Lu, *Chem. Sci.* **2024**, *15*, 8265

[41] H. Liu, Y. Geng, Z. Xiao, L. Ding, J. Du, A. Tang, E. Zhou, *Adv. Mater.* **2024**, *36*, 2404660.

[42] H. Chen, H. Liang, Z. Guo, Y. Zhu, Z. Zhang, Z. Li, X. Cao, H. Wang, W. Feng, Y. Zou, L. Meng, X. Xu, B. Kan, C. Li, Z. Yao, X. Wan, Z. Ma, Y. Chen, *Angew. Chem. Int. Ed.* **2022**, *61*, e202209580

[43] Y. Jiang, Y. Li, F. Liu, W. Wang, W. Su, W. Liu, S. Liu, W. Zhang, J. Hou, S. Xu, Y. Yi, X. Zhu, *Nat. Commun.* **2023**, *14*, 5079.

[44] Y. Shi, Y. Chang, K. Lu, Z. Chen, J. Zhang, Y. Yan, D. Qiu, Y. Liu, M. A. Adil, W. Ma, X. Hao, L. Zhu, Z. Wei, *Nat. Commun.* **2022**, *13*, 3256.

[45] W. Wei, C. Zhang, Zhan. Chen, W. Chen, G. Ran, G. Pan, W. Zhang, P. Buschbaum, Z. Bo, C. Yang, Z. Luo, *Angew. Chem. Int. Ed.* **2024**, *63*, e202315625.

[46] H. Lu, D. Li, W. Liu, G. Ran, H. Wu, N. Wei, Z. Tang, Y. Liu, W. Zhang, Z. Bo, *Angew. Chem. Int. Ed.* **2024**, *63*, e202407007.

[47] Z. Wang, M. Ji, A. Tang, M. Du, C. Mu, Y. Liu, E. Wang, E. Zhou, *Energy Environ. Sci.* **2024**, *17*, 3868.

[48] H. Liang, X. Bi, H. Chen, T. He, Y. Lin, Y. Zhang, K. Ma, W. Feng, Z. Ma, G. Long, C. Li, B. Kan, H. Zhang, O. A. Rakitin, X. Wan, Z. Yao, Y. Chen, *Nat. Commun.* **2023**, *14*, 4707.

[49] M. Xie, Y. Shi, L. Zhu, J. Zhang, Q. Cheng, H. Zhang, Y. Yan, M. Zhu, H. Zhou, K. Lu, Z. Wei, *Energy Environ. Sci.* **2023**, *16*, 3543.

[50] Z. Luo, W. Wei, R. Ma, G. Ran, M. H. Jee, Z. Chen, Y. Li, W. Zhang, H. Y. Woo, C. Yang, *Adv. Mater.* **2024**, *36*, 2407517.

[51] S. M. Cybulski, C. E. Seversen, *J. Chem. Phys.* **2005**, *122*, 014117.

[52] Y. Li, H. Fu, Z. Wu, X. Wu, M. Wang, H. Qin, F. Lin, H. Y. Woo, A. K. Jen, *ChemSusChem* **2021**, *14*, 3579.

[53] Q. Zhao, J. Liu, H. Wang, M. Li, K. Zhou, H. Yang, Y. Han, *J. Mater. Chem. C* **2015**, *3*, 8183.

[54] Y. Tamai, Y. Murata, S. −i. Natsuda, Y. Sakamoto, *Adv. Energy Mater.* **2024**, *14*, 2301890.

[55] T. A. Dela Peña, R. Ma, Y. Luo, Z. Xing, Q. Wei, Y. Hai, Y. Li, S. A. Garcia, K. L. Yeung, T. Jia, K. S. Wong, H. Yan, G. Li, M. Li, J. Wu, *Adv. Energy Mater.* **2024**, *14*, 2303169.

[56] X. Xie, R. Ma, Y. Luo, T. A. Dela Peña, P. W.-K. Fong, D. Luo, H. T. Chandran, T. Jia, M. Li, J. Wu, A. K. K. Kyaw, G. Li, *Adv. Energy Mater.* **2024**, *14*, 2401355.

[57] Y. Xu, H. Yao, L. Ma, L. Hong, J. Li, Q. Liao, Y. Zu, J. Wang, M. Gao, L. Ye, J. Hou, *Angew. Chem. Int. Ed.* **2020**, *59*, 9004.

[58] Y. Cui, P. Zhu, H. Hu, X. Xia, X. Lu, S. Yu, H. Tempeld, R. A. Eichel, X. Liao, Y. Chen, *Angew Chem. Int. Ed.* **2023**, *62*, e202304931.

[59] M. K. Etherington, J. Gibson, H. F. Higginbotham, T. J. Penfold, A. P. Monkman, Nat. Commun. **2016**, *7*, 13680.

[60] H. Noda, X. K. Chen, H. Nakanotani, T. Hosokai, M. Miyajima, N. Notsuka, Y. Kashima, J. L. Bredas, C. Adachi, *Nat. Mater.* **2019**, *18*, 1084.

[61] X.-K. Chen, D. Qian, Y. Wang, T. Kirchartz, W. Tress, H. Yao, J. Yuan, M. Hülsbeck, M. Zhang, Y. Zou, Y. Sun, Y. Li, J. Hou, O. Inganäs, V. Coropceanu, J. −L. Bredas, F. Gao, *Nat. Energy* **2021**, *6*, 799.

[62] S. Pang, Z. Wang, X. Yuan, L. Pan, W. Deng, H. Tang, H. Wu, S. Chen, C. Duan, F. Huang, Y. Cao, *Angew. Chem. Int. Ed.* **2021**, *60*, 8813.

TOC

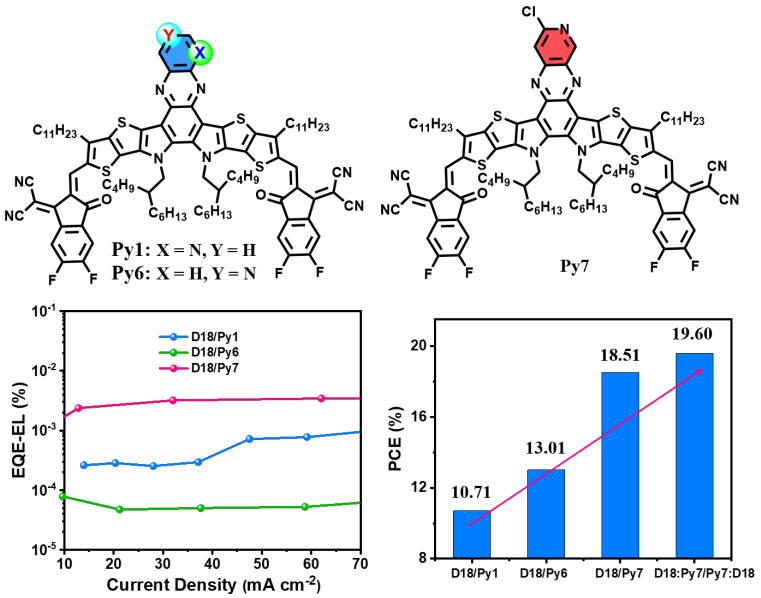

We present two new acceptors with pyrido[3,4-*b*]quinoxaline as electron-deficient component, namely Py6 and Py7. The D18/Py7 device yields higher efficiency of 18.51% than Py1- and Py6-based device due to the better morphology and low energy loss. Furthermore, the (D18:1wt% Py7)/(Py7:1wt% D18) device delivers a remarkable PCE of 19.60%.